Advanced Devices & Instrumentation
A SCIENCE PARTNER JOURNAL

REVIEW ARTICLE

Transparent Ultrasound Transducers: From Materials to Applications

Jiaming Zhang[1], Guocui Bao[1], Shilin Hou[1], Fan Yang[1], Guo Li[2], and Jiyan Dai[1]*

[1]Department of Applied Physics, The Hong Kong Polytechnic University, Hong Kong, Hong Kong. [2]School of Automation, Xi'an University of Posts & Telecommunications, Xi'an, China.

*Address correspondence to: jiyan.dai@polyu.edu.hk

Citation: Zhang J, Bao G, Hou S, Yang F, Li G, Dai J. Transparent Ultrasound Transducers: From Materials to Applications. *Adv. Devices Instrum.* 2025;6:Article 0083. https://doi.org/10.34133/adi.0083

Submitted 31 July 2024
Revised 1 November 2024
Accepted 4 November 2024
Published 1 April 2025

Ultrasound transducers are essential components for photoacoustic imaging (PAI) detection, which has high imaging depth and high contrast. Since conventional ultrasound transducers are opaque, complicated and bulky system designs are usually required for PAI utilizing different light and acoustic paths. To overcome the problem, transparent ultrasound transducers are highly desired, as light can transmit through transducers directly for easy alignment of light and acoustic wave. Recently, various types of transparent ultrasound transducers have been investigated for high-quality PAI. In this review, different transparent ultrasound transducers based on transparent piezoelectric materials are reviewed. Additionally, further improvement of transparent ultrasound transducers by optimization of structures of designs is discussed, and their potential applications are also discussed.

Introduction

Photoacoustic imaging (PAI) is a noninvasive biomedical imaging tool that combines the advantages of high penetration of ultrasound imaging and high contrast of optical imaging. PAI has now been widely used for lesion detection [1,2], vasculature imaging [3,4], and cancer detection/diagnosis [5,6]. Currently, there are 3 main kinds of PAI: photoacoustic computed tomography (PACT), photoacoustic microscopy (PAM), and photoacoustic endoscopy (PAE). The method of PAI signal of these 3 approaches is the same: Biological tissues are illuminated by pulsed laser with safe laser energy, and the energy of laser is absorbed by tissues being heated. During the periodic heating process, acoustic waves are generated due to thermoelastic effect, and ultrasound sensors are employed to detect these high-frequency acoustic waves. PAM and PAE usually use a ultrasound sensor with scanning for image acquisition, while PACT requires specific algorithms, such as universal back projection algorithm, to form image [7]. For PACT, the spatial resolution of image is determined by the ultrasound sensor; higher center frequency and broader bandwidth result in better resolution. Axial resolution of PAM and PAE is also highly related to characteristics of ultrasound sensor, while the lateral resolution depends on focal zones of laser and acoustic wave. Ultrasound sensors with high receiving sensitivity are usually desired for PAI for better image quality. Conventional ultrasound transducers usually consist of Cr/Au electrode and mixture of epoxy with metal/oxide powders, which are opaque and may block the light path [8,9]. Optical and acoustic designs are employed to achieve light illumination from sides for co-axial detection through reflection mode (Fig. 1A). This design inevitably results in bulky systems and inefficient signal detection. Transmission-mode PAI system may overcome this problem by allowing light illumination through opposite sides of the sample with appropriate design of acoustic detection (Fig. 1B). However, this design may not be suitable for practical in vivo applications, as light may be scattered in biological samples and cannot transmit through thick tissues. To partially solve this problem, a ring-shaped or hollow structure ultrasound transducers have been employed (Fig. 1C), where light can transmit through the central hole [10,11]. However, the central orifice may destroy structure of the transducer, leading to degraded performance [12]. Therefore, signals arriving at the place of central orifice may not be acquired, leading to further degraded imaging quality.

Allowing light transmission through the sensor directly may be an alternative way to co-align light and acoustic beam. This approach may achieve a simple system design and more effective signal acquisition (Fig. 1D). Transparent pure-optical ultrasound detection sensors, such as Fabry–Pérot sensor, have been investigated a lot in recent years [13,14]. Although these sensors possess advantages including broadband and sensitive detection, it is still challenging to make a parallel array; this substantially limits their implementation. Moreover, it is difficult to integrate these kinds of sensors into ultrasound/photoacoustic dual-modality imaging system. In this circumstance, transparent transducers were raised, which can be divided into 3 categories: transparent capacitive micromachined ultrasound transducer (CMUT) [15,16], transparent piezoelectric micromachined ultrasound transducers (PMUTs) [17,18], and piezoelectric transparent ultrasound transducers (TUTs). Among these transducers, TUT can not only be operated at high frequencies (>20 MHz) without any additional components but also be manufactured with low cost.

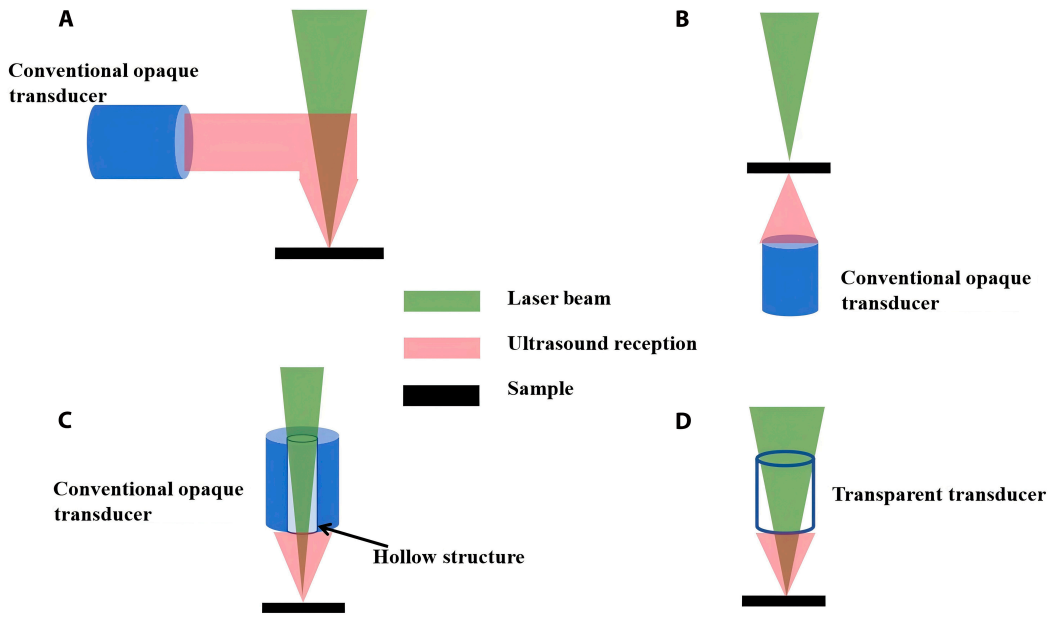

Fig. 1. (A) Reflection mode PAI system. (B) Reflection mode PAI system. (C) PAI system with a ring-shaped or hollow structure ultrasound transducer. (D) PAI system with a TUT.

The aim of this review is to provide an overview on reported TUTs, focusing on characteristics of transducers including piezoelectric materials and matching/backing layers. Challenges and future directions on development of TUT will also be discussed.

Lithium Niobate-Based TUT

The y-cut 36° lithium niobate (LN) has been studied a lot for transducer applications due to its high electromechanical coupling coefficient, low dielectric loss, and dielectric constant. With transparent nature, LN was firstly and widely studied for development of TUTs. Dangi et al. [19] demonstrated the LN-based TUTs with 14.5-MHz center frequency for PAE and PAM applications. Transparent indium tin oxide (ITO) electrodes were sputter deposited to supersede conventional Cr/Au electrodes, while transparent epoxy was used as backing layer; this process results in transparency over 80%. Although the bandwidth was limited (<30%) due to the lack of matching layers, photoacoustic A-line and phantom imaging were successfully achieved. Further investigation was conducted to apply this type of TUT for ex vivo optical-resolution PAM, where imaging capability of biological tissues was demonstrated (Fig. 2A) [20]. Dual-function TUT device was also investigated with a gradient-index (GRIN) lens bonded at the backside of LN for laser coupling (Fig. 2B). The compact design achieved PAI with 40-MHz center frequency and photoacoustic flow cytometry [21]. To enhance acoustic signal transmission efficiency, vapor-deposited parylene C was added in the front layer of TUT as a single matching layer. With improved sensitivity and bandwidth (~36%), TUT could be employed for awake mouse braining PAI. In addition, TUT may replace glass window during imaging [22]. Chen et al. [23] proposed a high-frequency TUT with similar structure, reaching 36.9-MHz center frequency and slightly improved bandwidth (~35%). With an additional layer, the transparency was not degraded. The high frequency was desired for in vivo PAI due to better axial resolution. Similarly, transparent epoxy, which possesses higher acoustic impedance compared to parylene C, was also considered as a matching layer material to further improve performance of TUT. Liao et al. [24] developed a large-aperture TUT with epoxy matching layer, where the large aperture provides relatively large field of view (FOV) so that the laser scanning method may be applied to improve the imaging speed (100 Hz over 1 mm). With clearly imaged microvascular network of mouse ear and abdomen, the ability of TUT for fast imaging and large organ imaging was demonstrated. Except for working as a matching layer, the transparent epoxy can also be filled as acoustic lens due to its low viscosity. A lens-focused TUT was developed for acoustic resolution PAM application [25], and the sensitivity of this TUT was increased with 2-way insertion loss as high as 17.12 dB at its center frequency. With this TUT, simultaneous ultrasound/PAI was then achieved for mouse in vivo (Fig. 2C).

However, the bandwidth of these TUTs was still narrow due to improper acoustic matching with low impedance matching layer of transparent polymer materials. Among all transparent polymer materials, polymethyl methacrylate (PMMA) has the highest acoustic impedance, which may be employed as the single transparent matching layer [26]. Through careful design with this matching scheme, 20- and 30-MHz TUTs were fabricated with 50% bandwidth (Fig. 2D) [27], where the effective electromechanical coefficient was increased to 0.6, and the axial resolution of the PAI achieved 111 μm. In vivo optical-resolution PAM was developed based on TUT, where the improved axial resolution was demonstrated. Nevertheless, the acoustic impedance of transparent polymer matching layer is still relatively low; this cannot solve the acoustic mismatch problem between LN and biological tissue effectively. As a common transparent material with high acoustic impedance, glass (>12 MRayl) was considered as the first matching layer for double matching layer scheme, and as reported, the bandwidth of the transducer has been increased to over 60% [28]. Except for glass, parylene C was also deposited as the second matching layer (Fig. 2E).

However, the broad bandwidth may be led by an additional low-frequency waveform, which was introduced by mass-load

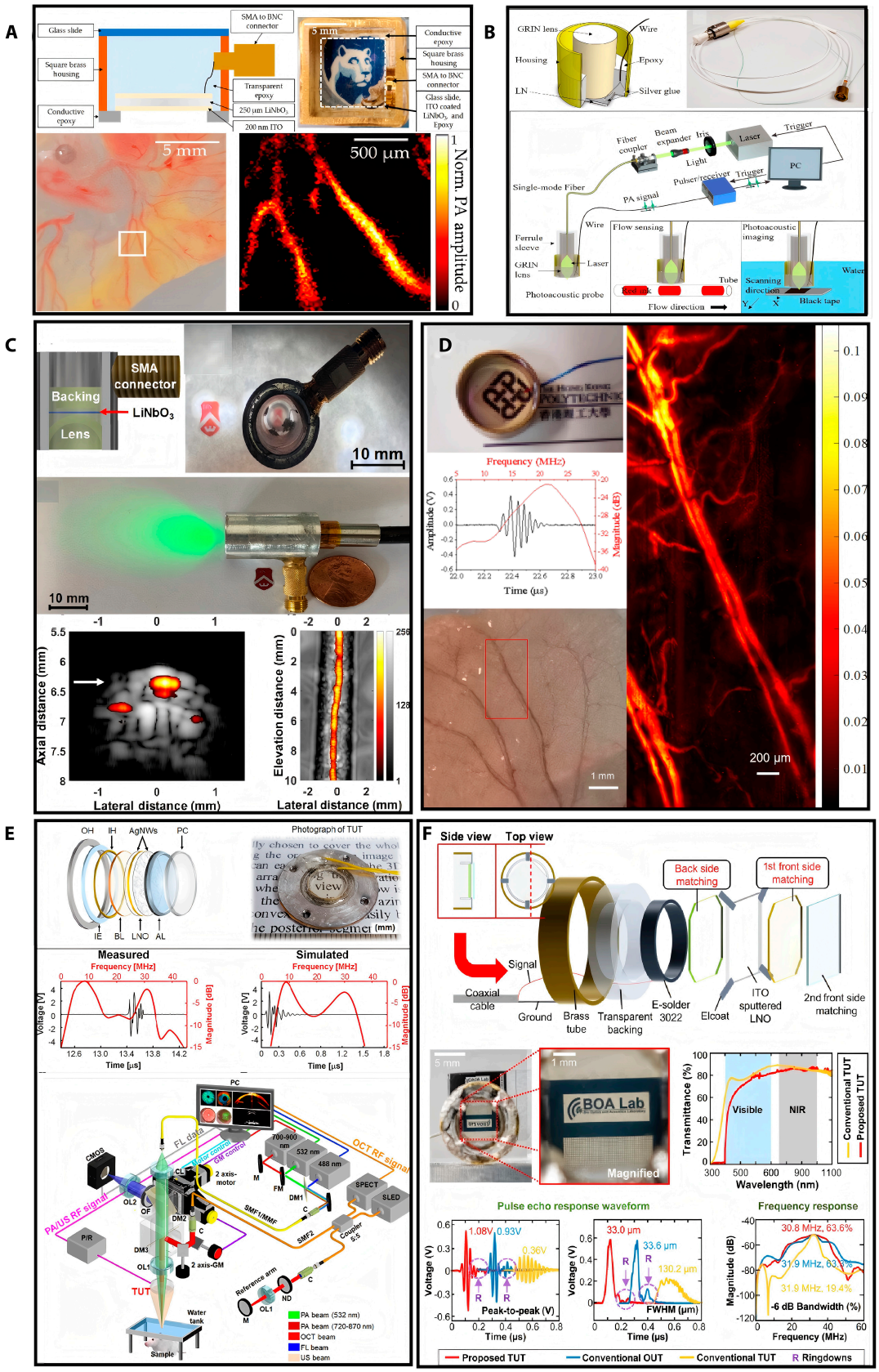

Fig. 2. (A) Schematic and photograph of TUT; photograph and PAI of chick-embryo chorioallantois membrane (CAM) [20]. (B) Schematic and photograph of developed TUT probe; schematics of system and experimental setup [21]. (C) Schematic and photograph of developed TUT and light propagation through TUT; in vivo photoacoustic/ultrasound imaging [25]. (D) Photograph of developed TUT; measured pulse-echo response and in vivo PAI imaging of mouse ear [27]. (E) Schematic and photograph of developed TUT; schematic diagram of developed quadruple imaging system based on TUT [29]. (F) Schematic and photograph of developed TUT; comparison of TUT with conventional transducer [34].

effect. Two measured center frequencies were reported as 7.2 and 11.8 MHz, while corresponding bandwidths were 36.1% and 62.7%, respectively. Similar phenomenon was also observed by Park et al. [29]. In their work, an acoustic lens was lapped down to a desired thickness and bonded as the first matching layer with parylene C as the second matching layer; this design of transducer results in 7.5- and 31.5-MHz center frequencies with 175% and 25.4% bandwidths, respectively. The measured axial resolutions of ultrasound imaging and PAI with this transducer were 890 and 91 μm, respectively. Quadruple biomedical imaging system, including ultrasound, PAI, optical coherence, and fluorescence, was developed based on TUT. This study verified the ability of TUT implementing with other biomedical optical imaging, where in vivo imaging without label was demonstrated. Another study utilizing similar TUT structure with higher frequency was reported with glass acoustic lens and parylene C for matching layer [30]; the center frequency of this TUT was measured as 36.9 MHz with 18.3% bandwidth. With this TUT, a high-speed optical-resolution PAM system was established and verified by in vivo imaging. As reported, Park et al. [31,32] improved bandwidth of TUT to over 50% by modifying the thickness of parylene C. Moreover, novel transparent composite materials were investigated for proper acoustic matching. Glass beads/epoxy composites with different weight fraction were studied [33]. The acoustic impedance of composites may achieve an ideal value; however, the increased fraction of glass bead may lead to light scattering, which is not desired for PAI. Only 15% glass beads can be applied for practical PAI application with limited bandwidth. Researchers then found that mico-SiO_2/epoxy composites achieved both high transparency and proper acoustic impedance [34]. Based on SiO_2 bead of 3-μm partial size and epoxy with low viscosity, matching and backing layers were developed to make a TUT whose performance was comparable to conventional opaque transducers (Fig. 2F). The ultrasensitive TUT results in high-quality ultrasound/PAI for both in vivo animal and human. Except for single-element TUT, transparent linear array was also investigated [35]. Although the performance of array element was degraded due to the sub-dicing LN stack, successful beamforming has been achieved, and phantom imaging was also successfully demonstrated to show effectiveness of this novel design.

Relaxor-PT Single Crystal-Based TUT

With the development of TUTs, investigations on matching and backing layers have gained many progresses. To further enhance performance of TUT, attentions on transparent piezoelectric layer should be paid. With carefully lapping and polishing, <001> direction lead magnesium niobate-lead titanate (PMN-PT) with the conventional DC poling method achieved transparency over 70% at specific wavelength (Fig. 3) [36]. With glass acoustic lens and parylene C for acoustic matching, a handheld photoacoustic finder-based TUT was developed with 8-MHz center frequency and 45% bandwidth. Moreover, a high-frequency TUT based on PMN-PT with optimized thickness double matching layer was developed for endoscopy application. The bandwidth could reach 50%, while high-quality ultrasound/PAI was successfully demonstrated for rectum and vagina of the rat in vivo [37].

With further investigation, researchers found that AC electric field can improve transparency and piezoelectricity simultaneously. With conventional DC electric field poling, the 109-degree domain wall and the 71-degree domain wall were observed. For AC poling, the domain size became larger, and during the

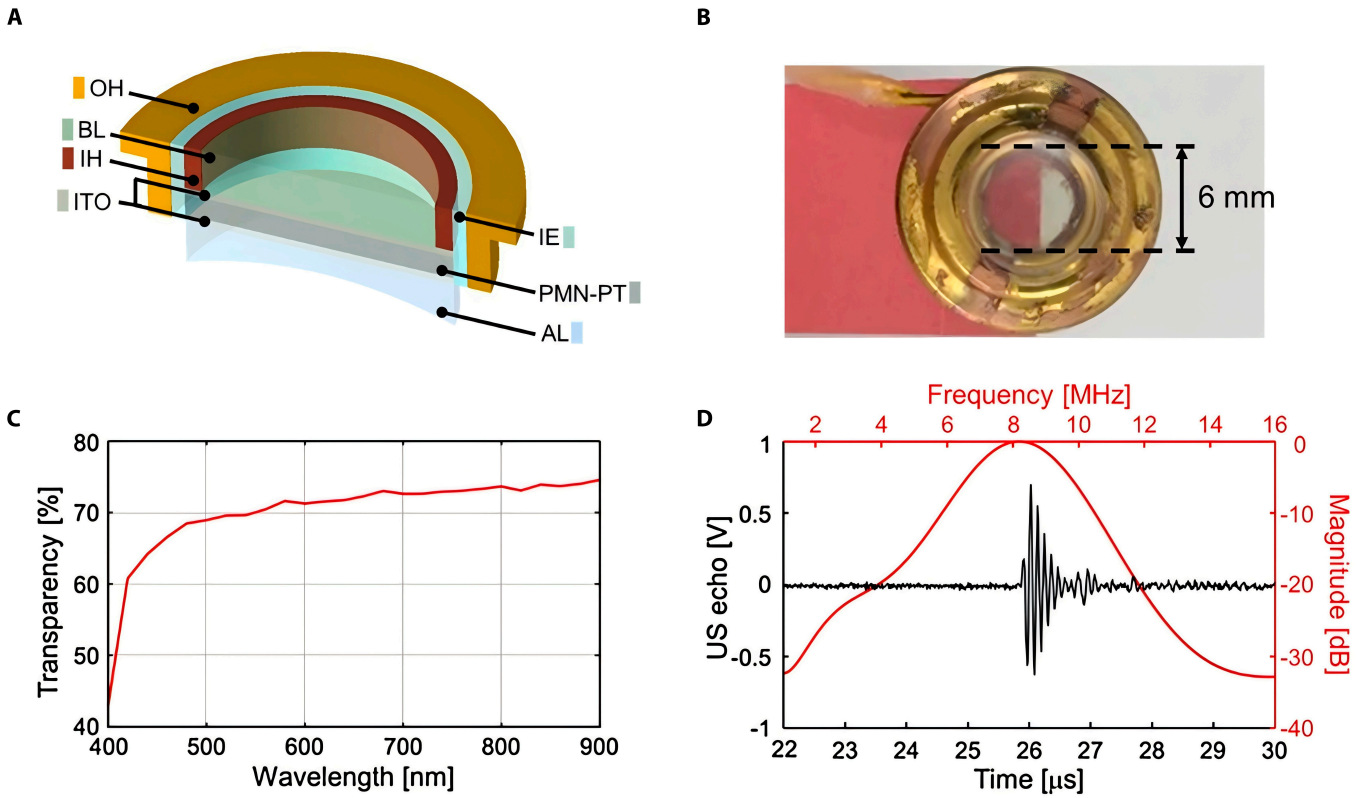

Fig. 3. (A) Schematic of proposed TUT and (B) photograph of TUT. (C) Measured transparency of TUT. (D) Measured pulse-echo response and frequency spectrum of TUT [36].

process, 71-degree domain walls were removed by AC electric field; in contrast to the 71-degree domain walls, the density of 109-degree walls remained unchanged. Because of the elimination of 71-degree walls, the AC poling process makes crystals more transparent and 30% enhancement of piezoelectricity [38]. A study was conducted to show the advantages of AC-poled PMN-PT compared to LN [28], where the AC-poled PMN-PT-based TUT was demonstrated to have both higher sensitivity and axial resolution compared to LN-based TUT.

Ceramic-Based TUT

As a common piezoelectric material, ceramics play important roles in transducer fabrication. Conventional piezoelectric ceramics, such as PZT, were always opaque due to their polycrystalline nature. Recently developed rare-earth element-doped lead titanate (PT)-based ceramics not only show comparable piezoelectric properties to single crystal [39] but also result in decreased domain size from micrometers to nanometers due to the doping; this gives rise to potentials of transparency [40]. In the aspect of microstructure, potential symmetric structure also enables PT-based ceramics to be transparent [41]. However, the grain boundaries and residual pores block the transparency of ceramics. The hot-press sintering method is an effective and unique way to solve the problem [42]. For instance, Eu-doped PMN-PT ceramic was sintered under 100-MPa pressure and 1,200 °C to achieve nearly 70% light transmittance, while d_{33} and dielectric constant were 1,400 pC/N and 13,300, respectively [43]. Eu-doped PMN-PT transparent piezoelectric ceramic has been investigated for high-frequency TUT applications (Fig. 4), and ultrasound/PAI was successfully demonstrated [44]. The transparent ceramics with both high d_{33} and dielectric constant possess great potential for miniaturize TUT application, such as endoscopy and intravascular PAI. Similar phenomenon was also investigated for lead-free ceramics. $K_xNa_{1-x}NbO_3$ (KNN) ceramics have achieved satisfied transparency (74%) with La doping [45].

Researchers also investigated TUT fabricated by the advanced 3D printing method with Er-doped $Li_{0.04}(K_{0.49}Na_{0.51})_{0.96}]NbO_3$ (KNNLN) ceramic powder. Through stereolithography technique, the transparent piezoelectric stack was printed, and then transparent epoxy was casted as the matching layer. The such made TUT shows 10.5-MHz center frequency and 18% bandwidth, and the photoacoustic signal can be successfully detected [46].

Polymer-Based TUT

Compared to single crystals and ceramics, piezoelectric polymers possess relatively lower acoustic impedance (<4 MRayl)

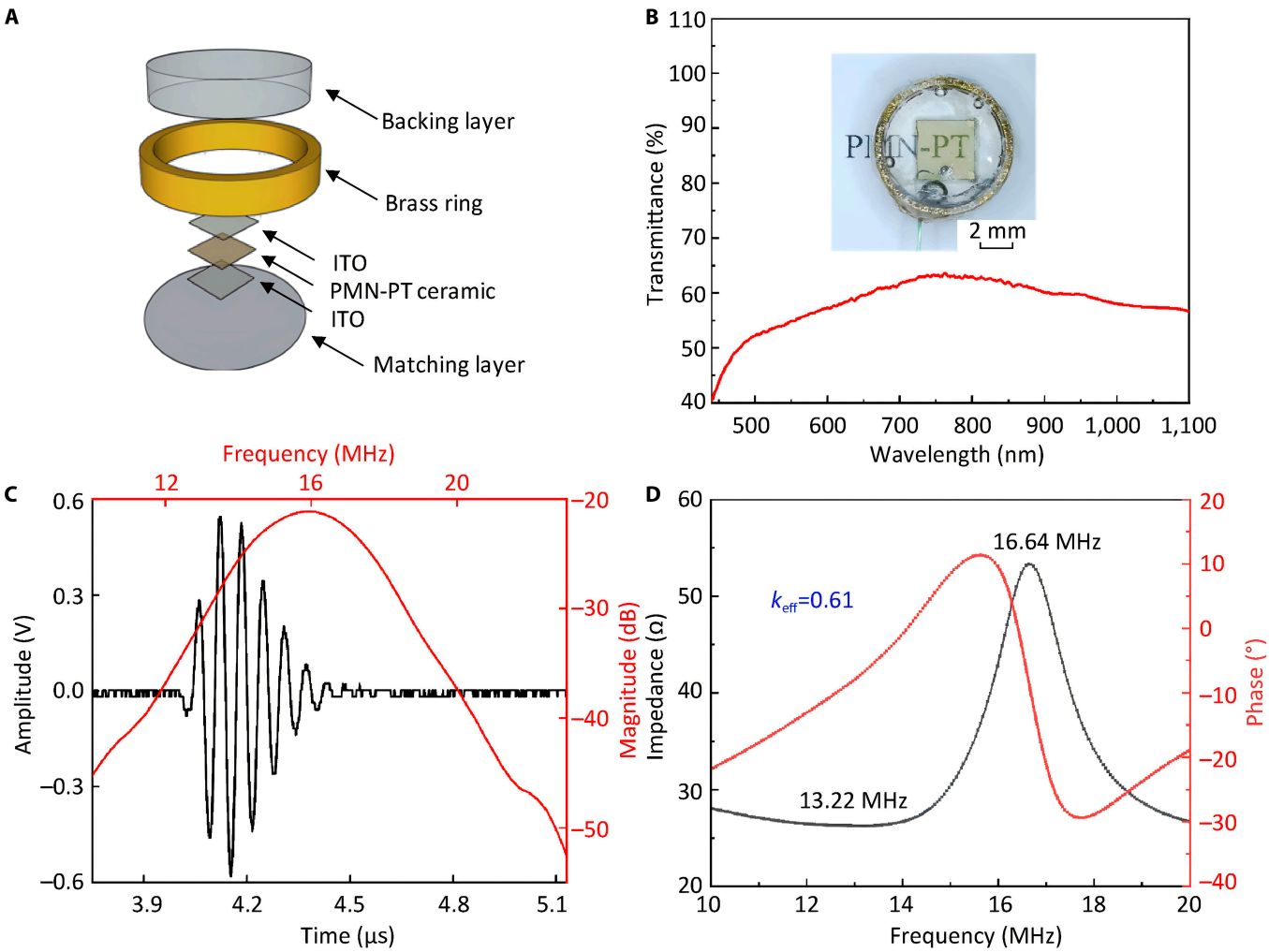

Fig. 4. (A) Exploded view of Eu-PMN-PT-based TUT. (B) Transmittance spectrum and photograph of TUT. Measured pulse-echo response, frequency spectrum (C), and impedance-phase diagram (D) of TUT [44].

for better acoustic matching, which was desired for TUT due to limited transparent matching layer materials. Polyvinylidene fluoride (PVDF) was a common piezoelectric polymer with transparent nature and good flexibility and has been widely accepted as an acoustic receiver due to its high receiving ability. With sputtered ITO electrode, PVDF was employed to fabricate a focused TUT with ~60% optical transmittance for PAM application. The PVDF film was compressed and stretched onto a convex glass lens for focusing and backing layer as well of TUT. Over 100% bandwidth was obtained for the 24-MHz TUT without any matching layer, and the axial resolution could be improved to 14.81 μm [47]. Further optimization of TUT was conducted for higher numerical aperture and higher center frequency to improve imaging qualities [48]. Ultrasound/PAI was achieved for a mouse tail to evaluate performance of the compact TUT. Ultraviolet-transparent TUT was also demonstrated for resolving densely distributed cell nuclei that are indistinguishable otherwise (Fig. 5A). Compared to conventional opaque transducer-based ultraviolet PAM system, TUT provides better lateral solution [49].

Integrated with a pre-amplifier, an ultrasensitive PVDF-based TUT was developed for PAI detection [50]. The receiving sensitivity of TUT shows substantial advantage compared to a commercial hydrophone. Application on PAE of PVDF-based TUT was also investigated (Fig. 5B). It shows that, with a small aperture size, PAI signal can be acquired and phantom imaging has been demonstrated with wave front shaping functions [51,52]. Due to the relatively lower dielectric constant of PVDF, researchers have tried to develop TUT with large aperture size for optimized electrical matching. A 6.7-MHz TUT has been successfully fabricated with 20 mm × 20 mm FOV, and a 3-dimensional (3D) phantom was imaged to evaluate its capability for PAI [53]. Except for PVDF, the co-polymer piezoelectric poly(vinylidene fluorideco-trifluoroethylene) [P(VDF-TrFE)] material, possessing better piezoelectric properties compared with PVDF, was also implemented in TUT fabrication [54]. One can see that the P(VDF-TrFE)-based TUT presented higher transparency and much better sensitivity compared to PVDF-based TUT with similar transducer structure. The transparent array was also investigated with a fiber array bundled [55]. The 4.3-MHz array was designed as the concave structure for focused light illumination and acoustic detection. Phantom PAI evaluated the performance of the compact and miniaturized array design and great imaging depth.

Discussion and Perspective

TUT has raised great interest for PAI as it provides a way for easy alignment of laser and acoustic wave for co-axially detection. Nowadays, limited by transparency, only a few kinds of piezoelectric materials have been investigated for TUT design and fabrication. Properties of these transparent piezoelectric materials were concluded in Table 1. Piezoelectric polymers, including PVDF and P(VDF-TrFE), possess high receiving sensitivity and high flexibility to form a focused transducer. Moreover, the low acoustic impedance of these polymers could match well with biological issues, leading to high acoustic transmission coefficient and broad bandwidth. However, their electromechanical coefficients and d_{33} are low, limiting their capability for ultrasound imaging with high signal-to-noise ratio (SNR). They may only be applicable to specification applications where receiving-only is required. Nowadays, more efforts have been spent on simultaneous ultrasound/PAI [56], which provides more requirements for high-performance TUTs. In this condition, the novel AC-poled relaxor-PT single crystals hold great advantages for further development of TUT. Except for PMN-PT, other similar AC-poled single crystal, such as $Pb(In_{1/2}Nb_{1/2})O_3$-$Pb(Mg_{1/3}Nb_{2/3})O_3$-$PbTiO_3$ (PIN-PMN-PT), may also be employed. As a cutting-edge technology, conditions of AC poling are under debate [28,57,58], where key factors of AC poling, including numbers of cycles, amplitude of electric field, and frequency of AC field, should be carefully studied to find out the most optimized poling conditions. To avoid de-poling, the single crystal was always poled after fabrication. For transparent electrode, mainly ITO and silver nanowire can reach relatively low sheet resistance; therefore, the sheet resistance of electrode layer may need to be considered during the poling process. Also, rare-earth element-doped PT-based ceramics, which possess high dielectric constant, also

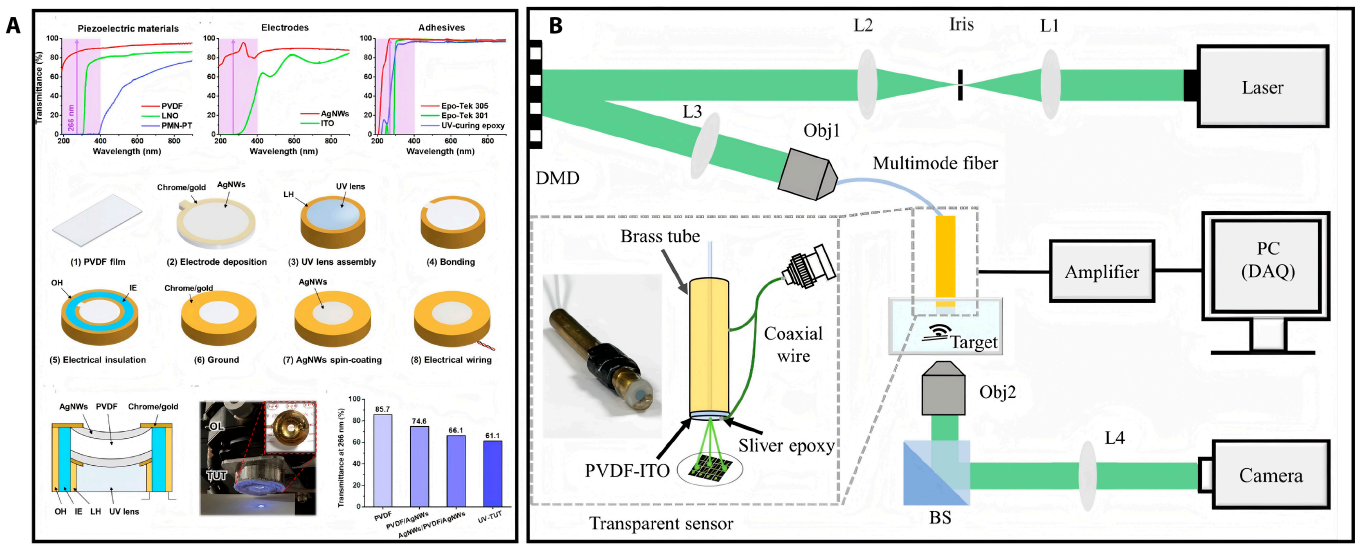

Fig. 5. (A) Properties of the developed TUT; schematic and photograph of TUT [49]. (B) Schematic of the imaging system; schematic and photograph of the developed endoscopy based on TUT [51].

hold potential for TUT with miniaturized aperture size for ultrasound/PAE imaging. Composite materials should also be studied for their improved electromechanical coupling coefficient and piezoelectric voltage constant.

In terms of TUT design, piezoelectric single crystals and ceramics have high acoustic impedance (>30 MRayl); therefore, carefully acoustic matching design is essential. Although PAI could be successfully demonstrated employing TUT without matching layer, the photoacoustic axial resolution of reported TUT is always low due to narrow bandwidth and low sensitivity. Table 2 summarizes bandwidth of reported TUT without or with single matching layer. Although polymer materials are transparent, their acoustic impedance is improper; therefore, the bandwidths of TUTs with these materials are not significantly improved due to their low acoustic impedance. Although PMMA with carefully adjusted thickness improved the bandwidth to 50%, the sensitivity of TUT is still limited with 28.4-dB insertion loss.

Double matching layer scheme results in better acoustic matching performance compared to that of single matching layer, and considering the acoustic impedance, glass may be a potential choice as the first matching layer. However, the heavy load of bonded glass may dampen the vibration of piezoelectric materials such that the actual (measured) frequency derives from the designated (theoretical) one. There have been studies of TUTs using glass as the quarter-wavelength-thick first matching layer and quarter-wavelength-thick parylene C as the second matching layer, but the bonded glass matching layer severely decreases the designated center frequency of transducers as indicated in Table 3. In theory, the implementation of a matching layer exhibiting the quarter-wavelength thickness results in an effective enhancement of the transducer's bandwidth. However, the quarter-wavelength thickness design is suitable for the matching layer fabricated by vapor deposition or casting in which the matching layer can be attached onto the piezoelectric layer directly. Due to the physical characteristics of glass, another alternative approach should be employed involving lapping glass to the desired thickness and then bond onto the surface of piezoelectric layer using a bonding agent. Nevertheless, different from the casting method, the thickness of bonding agent cannot be ignored, since it may influence the propagation of ultrasonic signal. Some studies even showed that the resonance mode was suppressed and changed into a dual-frequency resonance, which was undesired from the viewpoint of working principle of transducer technology. The phenomenon also hindered the development of high-frequency TUTs. For the dual-frequency transducers due to the bonding of quarter-wavelength thick heavy matching layer, the heavy load may not only decrease the vibration frequency of piezoelectric material but also introduce the low-frequency signal because of the mass-load effect. Although the low-frequency signal introduced could improve the bandwidth of pulse-echo signal, it may not contribute to the practical imaging applications as the superposition of 2 signals extends the pulse length. In theory, the axial resolution of ultrasound imaging is highly related to bandwidth of transducer. However, the axial resolution measured from imaging cannot match well with the theoretical value calculated

Table 1. Properties of transparent piezoelectric materials for TUTs

Piezoelectric material	Piezoelectric constant (d_{33}) (pC/N)	Dielectric constant	Electromechanical coefficient (k_t)
PVDF	20	20	0.2
P(VDF-TrFE)	36	16	0.3
LN	39	65	0.5
DC-poled PMN-PT single crystal	1,400	5,800	0.58
AC-poled PMN-PT single crystal	2,200	7,800	0.58
Eu-doped PMN-PT ceramic	1,400	13,300	0.62
3D-printed Er-doped KNNLN	97	/	0.36

Table 2. Bandwidth of reported transparent ultrasound transducers without or with a single matching layer

Center frequency (MHz)	Bandwidth (%)	Matching layer	Theoretical PAI axial resolution (μm)	Measured PAI axial resolution (μm)	Reference
13	25	/	169	150	[20]
36.9	33.9	Parylene C	105.9	105	[23]
10	16.46	EPO-TEK 301-2	782.5	/	[24]
13	36	Parylene C	282.1	202.5	[22]
11.93	22.43	15% volume fraction glass beads/epoxy	316	149.3	[33]
20	50	PMMA	126	111	[27]

Table 3. Performance of reported TUTs with double matching layers

Piezoelectric material	Center frequency (MHz)	BW (%)	First matching layer	Second matching layer	Theoretical PAI axial resolution (μm)	Measured PAI axial resolution (μm)	Reference
LN (250 μm)	7.2/11.8	36.1/62.7	Glass (100 μm)	Parylene C (40 μm)	/	375.9	[28]
AC-poled PMN-PT (200 μm)	7.8/13.2	28.2/66.67	Glass (100 μm)	Parylene C (40 μm)	/	285.6	[28]
LN (130 μm)	7.5/31.5	200/25.4	Glass lens	Parylene C (21 μm)	/	91	[29]
DC-poled PMN-PT (400 μm)	8	45	Glass lens	Parylene C (5 μm)	/	/	[36]
LN (250 μm)	6	50	Glass (100 μm)	Parylene C	/	/	[32]
LN (250 μm)	13	60	Glass (100 μm)	Parylene C (10 μm)	/	/	[31]
LN (100 μm)	34	18.3	Glass lens	Parylene C (10 μm)	215	208	[30]
PMN-PT	28.1	51.5	Glass	Parylene C		45	[37]

from the broad bandwidth. As indicated by researchers, although both the pulse-echo response and photoacoustic A-line showed the improved bandwidth, the axial resolution was reduced when compared to the previous work based on a TUT with no matching layer [20,28]. Thus, such design may not be applicable to the development of TUT for high-frequency or high-resolution application. Note that the reduction in the weight of the attached layer may improve the issue [33]; therefore, the thickness of bonded matching layer needs to be optimized instead of the traditional quarter-wavelength design. Researchers tried to adjust the thicknesses of matching layer materials such as glass (the first matching layer) and parylene (the second matching layer) as summarized in Table 3.

Although the thickness of parylene was adjusted to avoid the drop of center frequency, the same strategy did not work to achieve higher frequency in the subsequent work. Later on, the thickness of glass was carefully adjusted instead of quarter-wavelength thick. However, the approach may only work for developing transducers with a specific frequency. Transparent matching layer with low viscosity was investigated to solve the problem by casting it onto piezoelectric layer before curing. Although the broad-bandwidth and high-sensitivity TUT-based high-resolution PAI system has been successfully developed, the fabrication process is complex. For TUT with high frequency, it may bring extra risk of thin acoustic stack cracking. It is necessary to further study and investigate novel transparent matching layer with proper acoustic impedance and easier fabrication process. There are also studies focusing on transparent backing layer, which also influence the bandwidth of TUT. With improved transparent matching and backing layers, high-performance transparent arrays can be produced.

With the development of PAI, wearable and compact system designs have gained much interests [59,60]. TUTs help to minimize conventional PAI system as additional room for light path is not required. However, the image speed is limited. One reason is because of time of signal average, which could be solved by improved performance of TUT, especially sensitivity. The mechanical scanning method is also considered not fast enough, but TUT provides a simple laser scanning method. During imaging, the sample and transducer remain unmoved, while only laser spot transmitting through TUT moved with fast speed. Additionally, other biomedical optical technologies, such as photoplethysmography (PPG), were also studied to combine with ultrasound imaging due to development of TUTs. More studies need to be conducted for further investigation on fusion of ultrasound/PAI with other light-related healthcare monitoring technologies. Based on TUT, real-time and wearable ultrasound/PAI holds potential for unobtrusive sensing. It is expected that the applications of TUTs will bring significant improvements to all aspects of biomedical imaging area.

Acknowledgments

Funding: This work was supported by the National Key Research and Development Program of China (grant no. 2023YFC2410900), National Natural Science Foundation Grants of China (12104369), and Hong Kong General Research Fund (15220920).
Author contributions: Data curation: J.Z., G.B., S.H., F.Y., and G.L. Original manuscript draft: J.Z. Funding acquisition: G.L. and J.D. Review and editing: J.D. Supervision: J.D. All authors have read and agreed to the published version of the manuscript.
Competing interests: The authors declare that they have no competing interests.

Data Availability

Data are contained within the article.

References

1. Cheng R, Shao J, Gao X, Tao C, Ge J, Liu X. Noninvasive assessment of early dental lesion using a dual-contrast photoacoustic tomography. *Sci Rep*. 2016;6(1):21798.

2. Iskander-Rizk S, Kruizinga P, Beurskens R, Springeling G, Mastik F, de Groot NM, Knops P, van der Steen AF, van Soest G. Real-time photoacoustic assessment of radiofrequency ablation lesion formation in the left atrium. *Photoacoustics*. 2019;16:Article 100150.
3. Li S, Zhang G, Wang Y, Li W, Sun Y, Li C. Photoacoustic imaging of peripheral vessels in extremities by large-scale synthetic matrix array. *J Biomed Opt*. 2024;29(1 Suppl):S11519.
4. Sun Y, Wang Y, Li W, Li C. Real-time dual-modal photoacoustic and fluorescence small animal imaging. *Photoacoustics*. 2024;36:Article 100593.
5. Zhang G, Li W, Yang M, Li C. Developing a photoacoustic whole-breast imaging system based on the synthetic matrix array. *Front Phys*. 2020;8:Article 600589.
6. Han T, Yang M, Yang F, Zhao L, Jiang Y, Li C. A three-dimensional modeling method for quantitative photoacoustic breast imaging with handheld probe. *Photoacoustics*. 2021;21:Article 100222.
7. Xu M, Wang LV. Universal back-projection algorithm for photoacoustic computed tomography. *Phys Rev E*. 2005;71(1):Article 016706.
8. Cannata JM, Ritter TA, Chen W-H, Silverman RH, Shung KK. Design of efficient, broadband single-element (20-80 MHz) ultrasonic transducers for medical imaging applications. *IEEE Trans Ultrason Ferroelectr Freq Control*. 2003;50(11):1548–1557.
9. Li G, Sun Q, Fu Y, Hou S, Zhang J, Xu KL, Dai JY. A single crystal row–column-array for 3D ultrasound imaging. *Ultrasonics*. 2024;139:Article 107289.
10. Dangi A, Agrawal S, Lieberknecht J, Zhang J, Kothapalli S-R. Ring ultrasound transducer based miniaturized photoacoustic imaging system. Paper presented at: 2018 IEEE Sensors;2018; New Delhi, India.
11. Xiao J, Li Y, Jin W, Peng K, Zhu Z, Wang B. Photoacoustic endoscopy with hollow structured lens-focused polyvinylidine fluoride transducer. *Appl Opt*. 2016;55(9):2301–2305.
12. Lin R, Zhang Q, Lv S, Zhang J, Wang X, Shi D, Gong X, Lam KH. Miniature intravascular photoacoustic endoscopy with coaxial excitation and detection. *J Biophotonics*. 2023;16(4):Article e202200269.
13. Ren D, Sun Y, Shi J, Chen R. A review of transparent sensors for photoacoustic imaging applications. *Photonics*. 2021;8(8):324.
14. Ansari R, Zhang EZ, Desjardins AE, David AL, Beard PC. Use of a flexible optical fibre bundle to interrogate a Fabry–Perot sensor for photoacoustic imaging. *Opt Express*. 2019;27(26):37886–37899.
15. Peng H, Cheng Z, Zeng L, Ji X. Photoacoustic microscopy based on transparent piezoelectric ultrasound transducers. *J Innov Opt Health Sci*. 2023;16(05):2330001.
16. Li Z, Ilkhechi AK, Zemp R. Transparent capacitive micromachined ultrasonic transducers (CMUTs) for photoacoustic applications. *Opt Express*. 2019;27(9): 13204–13218.
17. Pavageau F, Dieppedale C, Perreau P, Liechti R, Hamelin A, Licitra C, Casset F, Le Rhun G. Highly transparent piezoelectric PZT membranes for transducer applications. *Sensors Actuators A Phys*. 2022;346:Article 113866.
18. Manwar R, Avanaki K. Manufacturing process of optically transparent ultrasound transducer: A review. *IEEE Sensors J*. 2023;23(8):8080–8093.
19. Dangi A, Agrawal S, Kothapalli S-R. Lithium niobate-based transparent ultrasound transducers for photoacoustic imaging. *Opt Lett*. 2019;44(21):5326–5329.
20. Chen H, Agrawal S, Dangi A, Wible C, Osman M, Abune L, Jia H, Rossi R, Wang Y, Kothapalli S-R. Optical-resolution photoacoustic microscopy using transparent ultrasound transducer. *Sensors*. 2019;19(24):5470.
21. Lin R, Zhang J, Gao W, Wang X, Lv S, Lam K-H, Gong X. A miniature multi-functional photoacoustic probe. *Micromachines*. 2023;14(6):1269.
22. Mirg S, Chen H, Turner KL, Gheres KW, Liu J, Gluckman BJ, Drew PJ, Kothapalli S-R. Awake mouse brain photoacoustic and optical imaging through a transparent ultrasound cranial window. *Opt Lett*. 2022;47(5):1121–1124.
23. Chen R, He Y, Shi J, Yung C, Hwang J, Wang LV, Zhou Q. Transparent high-frequency ultrasonic transducer for photoacoustic microscopy application. *IEEE Trans Ultrason Ferroelectr Freq Control*. 2020;67(9):1848–1853.
24. Liao T, Liu Y, Wu J, Deng L, Deng Y, Zeng L, Ji X. Centimeter-scale wide-field-of-view laser-scanning photoacoustic microscopy for subcutaneous microvasculature in vivo. *Biomed Opt Express*. 2021;12(5):2996–3007.
25. Park S, Kang S, Chang JH. Optically transparent focused transducers for combined photoacoustic and ultrasound microscopy. *J Med Biol Eng*. 2020;40:707–718.
26. Selfridge AR. Approximate material properties in isotropic materials. *IEEE Trans Sonics Ultrason*. 1985;32(3):381–394.
27. Zhang J, Long X, Zhang G, Ma Z, Li W, Wang Y, Yang F, Lin R, Li C, Lam K-H. Broadband transparent ultrasound transducer with polymethyl methacrylate as matching layer for in vivo photoacoustic microscopy. *Photoacoustics*. 2023;33:Article 100548.
28. Chen H, Mirg S, Osman M, Agrawal S, Cai J, Biskowitz R, Minotto J, Kothapalli S-R. A high sensitivity transparent ultrasound transducer based on PMN-PT for ultrasound and photoacoustic imaging. *IEEE Sens Lett*. 2021;5(11):1–4.
29. Park J, Park B, Kim TY, Jung S, Choi WJ, Ahn J, Yoon DH, Kim J, Jeon S, Lee D, et al. Quadruple ultrasound, photoacoustic, optical coherence, and fluorescence fusion imaging with a transparent ultrasound transducer. *Proc Natl Acad Sci USA*. 2021;118(11):Article e1920879118.
30. Chen M, Jiang L, Cook C, Zeng Y, Vu T, Chen R, Lu G, Yang W, Hoffmann U, Zhou Q, et al. High-speed wide-field photoacoustic microscopy using a cylindrically focused transparent high-frequency ultrasound transducer. *Photoacoustics*. 2022;28:Article 100417.
31. Park J, Park B, Yong U, Ahn J, Kim JY, Kim HH, Jang J, Kim C. Bi-modal near-infrared fluorescence and ultrasound imaging via a transparent ultrasound transducer for sentinel lymph node localization. *Opt Lett*. 2022;47(2):393–396.
32. Park J, Park B, Ahn J, Kim D, Kim JY, Kim HH, Kim C. Opto-ultrasound biosensor for wearable and mobile devices: Realization with a transparent ultrasound transducer. *Biomed Opt Express*. 2022;13(9):4684–4692.
33. Osman MS, Chen H, Creamer K, Minotto J, Liu J, Mirg S, Christian J, Bai X, Agrawal S, Kothapalli S-R. A novel matching layer design for improving the performance of transparent ultrasound transducers. *IEEE Trans Ultrason Ferroelectr Freq Control*. 2022;69(9):2672–2680.
34. Cho S, Kim M, Ahn J, Kim Y, Lim J, Park J, Kim HH, Kim WJ, Kim C. An ultrasensitive and broadband transparent ultrasound transducer for ultrasound and photoacoustic imaging in-vivo. *Nat Commun*. 2024;15(1):1444.
35. Chen H, Agrawal S, Osman M, Minotto J, Mirg S, Liu J, Dangi A, Tran Q, Jackson T, Kothapalli S-R. A transparent

ultrasound array for real-time optical, ultrasound, and photoacoustic imaging. *BME Front*. 2022;2022, 9871098.
36. Park B, Han M, Park J, Kim T, Ryu H, Seo Y, Kim WJ, Kim HH, Kim C. A photoacoustic finder fully integrated with a solid-state dye laser and transparent ultrasound transducer. *Photoacoustics*. 2021;23:Article 100290.
37. Kim J, Heo D, Park J, Cho S, Ahn J, Kim J, Ha M, Kim HH, Kim C. High-resolution photoacoustic and ultrasound endoscope based on the transparent ultrasound transducer. Paper presented at: SPIE BiOS; 2023; San Francisco, CA, USA.
38. Qiu C, Wang B, Zhang N, Zhang S, Liu J, Walker D, Wang Y, Tian H, Shrout TR, Xu Z, et al. Transparent ferroelectric crystals with ultrahigh piezoelectricity. *Nature*. 2020;577(7790):350–354.
39. Guo Q, Li F, Xia F, Gao X, Wang P, Hao H, Sun H, Liu H, Zhang S. High-performance Sm-doped $Pb(Mg_{1/3}Nb_{2/3})O_3$-$PbZrO_3$-$PbTiO_3$-based piezoceramics. *ACS Appl Mater Interfaces*. 2019;11(46):43359–43367.
40. Zheng F, Tian X, Fang Z, Lin J, Lu Y, Gao W, Xin R, Fu D, Qi Y, Ma Z, et al. Sm-doped PIN-PMN-PT transparent ceramics with high curie temperature, good piezoelectricity, and excellent electro-optical properties. *ACS Appl Mater Interfaces*. 2023;15(5):7053–7062.
41. Xiao Z, Yu S, Li Y, Ruan S, Kong LB, Huang Q, Huang Z, Zhou K, Su H, Yao Z, et al. Materials development and potential applications of transparent ceramics: A review. *Mater Sci Eng R Rep*. 2020;139:Article 100518.
42. Wang SF, Zhang J, Luo DW, Gu F, Tang DY, Dong ZL, Tan GEB, Que WX, Zhang TS, Li S, et al. Transparent ceramics: Processing, materials and applications. *Prog Solid State Chem*. 2013;41(1-2):20–54.
43. Yan P, Qin Y, Xu Z, Han F, Wang Y, Wen Z, Zhang Y, Zhang S. Highly transparent Eu-doped 0.72PMN-0.28PT ceramics with excellent piezoelectricity. *ACS Appl Mater Interfaces*. 2021;13(45):54210–54216.
44. Guo P, Gao W, Lin R, Wang X, Lan J, Zhang J, Wang Y, Zhu L, Zhang Y, Li F, et al. Advancement in PMN-PT transparent piezoelectric ceramic for photoacoustic/ultrasound dual-mode imaging. *J Mater*. 2024;11(4):Article 100932.
45. Yang D, Yang Z, Zhang X, Wei L, Chao X, Yang Z. High transmittance in lead-free lanthanum modified potassium-sodium niobate ceramics. *J Alloys Compd*. 2017;716:21–29.
46. Chen Y, Zhang D, Luo H, Peng Z, Zeng L, Yuan M, Ji X. 3D printed Er^{3+} doped KNNLN piezoelectric ceramics for transparent ultrasonic transducer application. *Ceram Int*. 2024;50(7):9979–9984.
47. Fang C, Hu H, Zou J. A focused optically transparent PVDF transducer for photoacoustic microscopy. *IEEE Sensors J*. 2019;20(5):2313–2319.
48. Fang C, Zou J. Acoustic-resolution photoacoustic microscopy based on an optically transparent focused transducer with a high numerical aperture. *Opt Lett*. 2021;46(13):3280–3283.
49. Kim D, Park E, Park J, Perleberg B, Jeon S, Ahn J, Ha M, Kim HH, Kim JY, Jung CK, et al. An ultraviolet-transparent ultrasound transducer enables high-resolution label-free photoacoustic histopathology. *Laser Photonics Rev*. 2024;18(2):2300652.
50. Liu Y-H, Kurnikov A, Li W, Kazakov V, Ni R, Subochev P, Razansky D. Sensitive ultrawideband transparent PVDF-ITO ultrasound detector for optoacoustic microscopy. *Opt Lett*. 2022;47(16):4163–4166.
51. Zhao T, Zhang M, Ourselin S, Xia W. Wavefront shaping-assisted forward-viewing photoacoustic endomicroscopy based on a transparent ultrasound sensor. *Appl Sci*. 2022;12(24):12619.
52. Zhao T, Ourselin S, Vercauteren T, Xia W. Miniaturized transparent ultrasound sensor for photoacoustic endoscopy. Paper presented at: Photons Plus Ultrasound: Imaging and Sensing 2022; 2022; San Francisco, CA, USA.
53. Liu Y-H, Chen L-X, Li C-Y, Lin F-S, Su H-Y, Tsai C-T, Wang L-W, Wang Y-H, Huang C-H. Transparent flexible piezoelectric ultrasound transducer for photoacoustic imaging system. *IEEE Sensors J*. 2021;22(3):2070–2077.
54. Fang C, Zhao Z, Fang J, Zou J. An optically-transparent focused P (VDF-TrFE) transducer for photoacoustic microscopy (PAM). *IEEE Sensors J*. 2023;23(12):12644–12650.
55. Hu H, Fang C, Zou J. An optically-transparent PVDF transducer array for photoacoustic tomography. Paper presented at: Photons Plus Ultrasound: Imaging and Sensing 2022; 2022; San Francisco, CA, USA.
56. Yu Y, Feng T, Qiu H, Gu Y, Chen Q, Zuo C, Ma H. Simultaneous photoacoustic and ultrasound imaging: A review. *Ultrasonics*. 2024;139:107277.
57. Guan Y, Hang H, Lin D, Wang X'a, Tang Y, Luo H. Enhancement of 10 MHz single element ultrasonic transducers based on alternating current polarized PIN-PMN-PT single crystals. *Sensors Actuators A Phys*. 2023;354:Article 114275.
58. Ma Z, Jia N, Li C, Ning L, Dang Y, Du H, Li F, Xu Z. Improved piezoelectric properties of 2–2 piezoelectric single crystal composites for acoustic transducer applications via alternating current polarization. *Mater Lett*. 2023;353:Article 135284.
59. Zhang T, Guo H, Qi W, Xi L. Wearable photoacoustic watch for humans. *Opt Lett*. 2024;49(6):1524–1527.
60. Tang J, Dai X, Jiang H. Wearable scanning photoacoustic brain imaging in behaving rats. *J Biophotonics*. 2016;9(6):570–575.

Advanced Devices & Instrumentation
A SCIENCE PARTNER JOURNAL

Transparent Ultrasound Transducers: From Materials to Applications

Jiaming Zhang, Guocui Bao, Shilin Hou, Fan Yang, Guo Li, and Jiyan Dai

Citation: Zhang J, Bao G, Hou S, Yang F, Li G, Dai J. Transparent Ultrasound Transducers: From Materials to Applications. *Adv Devices Instrum*. 2025;**6**:0083. DOI: 10.34133/adi.0083

Ultrasound transducers are essential components for photoacoustic imaging (PAI) detection, which has high imaging depth and high contrast. Since conventional ultrasound transducers are opaque, complicated and bulky system designs are usually required for PAI utilizing different light and acoustic paths. To overcome the problem, transparent ultrasound transducers are highly desired, as light can transmit through transducers directly for easy alignment of light and acoustic wave. Recently, various types of transparent ultrasound transducers have been investigated for high-quality PAI. In this review, different transparent ultrasound transducers based on transparent piezoelectric materials are reviewed. Additionally, further improvement of transparent ultrasound transducers by optimization of structures of designs is discussed, and their potential applications are also discussed.
Image

Advanced Devices & Instrumentation (ISSN 2767-9713) is published by the American Association for the Advancement of Science. 1200 New York Avenue NW, Washington, DC 20005.